Since January 2020 Elsevier has created a COVID-19 resource centre with free information in English and Mandarin on the novel coronavirus COVID-19. The COVID-19 resource centre is hosted on Elsevier Connect, the company's public news and information website.

Brief Report

Cell Host & Microbe

Increased resistance of SARS-CoV-2 variant P.1 to antibody neutralization

Graphical abstract

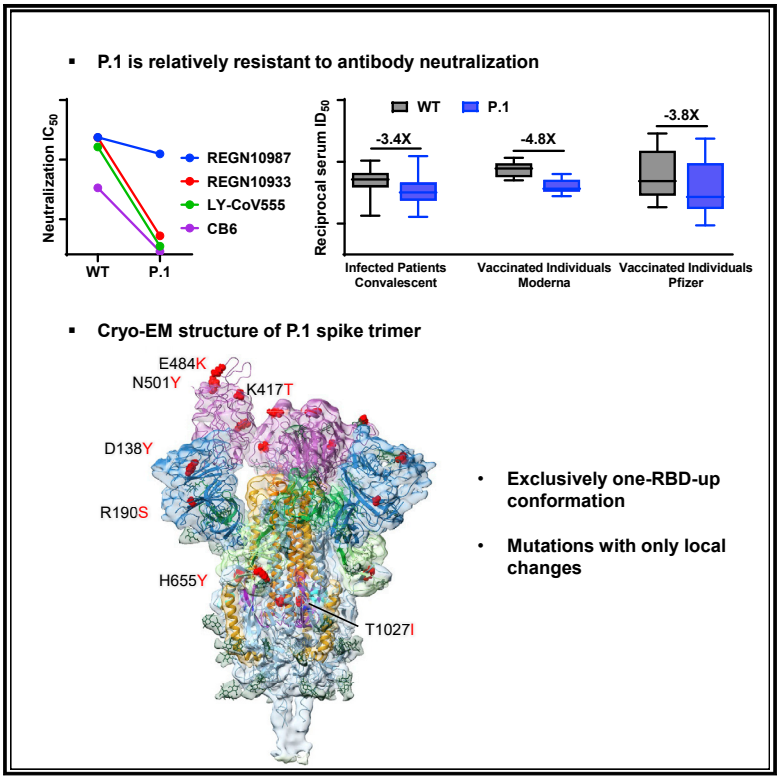

Highlights

- P.1 is refractory to multiple neutralizing mAbs, including three out of the four with EUA
- P.1 is relatively resistant to neutralization by convalescent plasma and vaccinee sera
- Cryo-EM structure of P.1 spike trimer reveals exclusively one-RBD-up conformation

Authors

Pengfei Wang, Ryan G. Casner, Manoj S. Nair, ..., Yaoxing Huang, Lawrence Shapiro, David D. Ho

Correspondence

pw2517@cumc.columbia.edu (P.W.), lss8@columbia.edu (L.S.), dh2994@cumc.columbia.edu (D.D.H.)

In brief

Wang et al. report that an emergent SARS-CoV-2 variant, P.1, is relatively resistant to neutralization by multiple therapeutic monoclonal antibodies, convalescent plasma, and vaccinee sera. The cryoelectron microscopy structure reveals the P.1 trimer to adopt exclusively a conformation with one of the receptor-binding domains in the "up" position.

Wang et al., 2021, Cell Host & Microbe *29*, 747–751
May 12, 2021
https://doi.org/10.1016/j.chom.2021.04.007

CellPress

Cell Host & Microbe

CellPress

Brief Report

Increased resistance of SARS-CoV-2 variant P.1 to antibody neutralization

Pengfei Wang,[1,6,*] Ryan G. Casner,[2,6] Manoj S. Nair,[1,6] Maple Wang,[1] Jian Yu,[1] Gabriele Cerutti,[2] Lihong Liu,[1] Peter D. Kwong,[2,3] Yaoxing Huang,[1] Lawrence Shapiro,[1,2,*] and David D. Ho[1,4,5,7,*]

[1]Aaron Diamond AIDS Research Center, Columbia University Vagelos College of Physicians and Surgeons, New York, NY 10032, USA
[2]Department of Biochemistry and Molecular Biophysics, Columbia University, New York, NY 10032, USA
[3]Vaccine Research Center, National Institute of Allergy and Infectious Diseases, National Institutes of Health, Bethesda, MD 20892, USA
[4]Department of Microbiology and Immunology, Columbia University Irving Medical Center, New York, NY 10032, USA
[5]Division of Infectious Diseases, Department of Internal Medicine, Columbia University Vagelos College of Physicians and Surgeons, New York, NY 10032, USA
[6]These authors contributed equally
[7]Lead contact
*Correspondence: pw2517@cumc.columbia.edu (P.W.), lss8@columbia.edu (L.S.), dh2994@cumc.columbia.edu (D.D.H.)
https://doi.org/10.1016/j.chom.2021.04.007

SUMMARY

The emergence of SARS-CoV-2 variants has raised concerns about altered sensitivity to antibody-mediated immunity. The relative resistance of SARS-CoV-2 variants B.1.1.7 and B.1.351 to antibody neutralization has been recently investigated. We report that another emergent variant from Brazil, P.1, is not only refractory to multiple neutralizing monoclonal antibodies but also more resistant to neutralization by convalescent plasma and vaccinee sera. The magnitude of resistance is greater for monoclonal antibodies than vaccinee sera and evident with both pseudovirus and authentic P.1 virus. The cryoelectron microscopy structure of a soluble prefusion-stabilized spike reveals that the P.1 trimer adopts exclusively a conformation in which one of the receptor-binding domains is in the "up" position, which is known to facilitate binding to entry receptor ACE2. The functional impact of P.1 mutations thus appears to arise from local changes instead of global conformational alterations. The P.1 variant threatens current antibody therapies but less so protective vaccine efficacy.

Severe acute respiratory syndrome coronavirus 2 (SARS-CoV-2) P.1, emerging from the B.1.1.28 lineage, has become a dominant variant in Brazil (Faria, 2021; Naveca, 2021). P.1 contains 10 spike mutations in addition to D614G, including K417T, E484K, and N501Y in the receptor-binding domain (RBD); L18F, T20N, P26S, D138Y, and R190S in the N-terminal domain (NTD); and H655Y near the furin cleavage site. This new variant could threaten the efficacy of current monoclonal antibody (mAb) therapies or vaccines because it shares mutations at the same three RBD residues with B.1.351, a variant that first emerged from South Africa (Tegally et al., 2021). We and others (Liu et al., 2021; Wang et al., 2021; Wu et al., 2021) have shown that B.1.351 is more resistant to neutralization by some mAbs, convalescent plasma, and vaccinee sera, in part due to a E484K mutation that also exists in P.1. We therefore obtained the P.1 authentic virus and also created, as previously described (Liu et al., 2020; Wang et al., 2020; Wang et al., 2021), a vesicular stomatitis virus (VSV)-based SARS-CoV-2 pseudovirus with all 10 mutations of the P.1 variant (BZΔ10), and assessed their susceptibility to neutralization by 18 neutralizing mAbs, 20 convalescent plasma, and 22 vaccinee sera as previously reported (Wang et al., 2021).

We first assayed the neutralizing activity of four mAbs with Emergency Use Authorization (EUA), including REGN10987 (imdevimab), REGN10933 (casirivimab) (Hansen et al., 2020), LY-CoV555 (bamlanivimab) (Chen et al., 2021; Gottlieb et al., 2021), and CB6 (etesevimab) (Gottlieb et al., 2021; Shi et al., 2020) against P.1 pseudovirus (BZΔ10) and authentic virus, alongside their wild-type (WT or WA1) counterparts. As shown in Figure 1A (left panel) and Figure S1A, the neutralizing activities of three of the mAbs with EUA were markedly or completely abolished against P.1. The only mAb with EUA retaining its activity was REGN10987. We next tested the neutralizing activity of eight additional RBD mAbs, including ones from our own collection (2-15, 2-7, 1-57, and 2-36) (Liu et al., 2020) as well as S309 (Pinto et al., 2020), COV2-2196 and COV2-2130 (Zost et al., 2020), and C121 (Robbiani et al., 2020). The neutralizing activities of the two potent mAbs targeting the receptor-binding motif, 2-15 and C121, were completely lost against P.1 (Figures 1A, middle panel; Figure S1A). Other mAbs targeting the "inner side" or the "outer side" of the RBD retained their activities against P.1, however. Overall, the data on pseudovirus and authentic virus were in agreement, and the findings on P.1 mimic those observed for

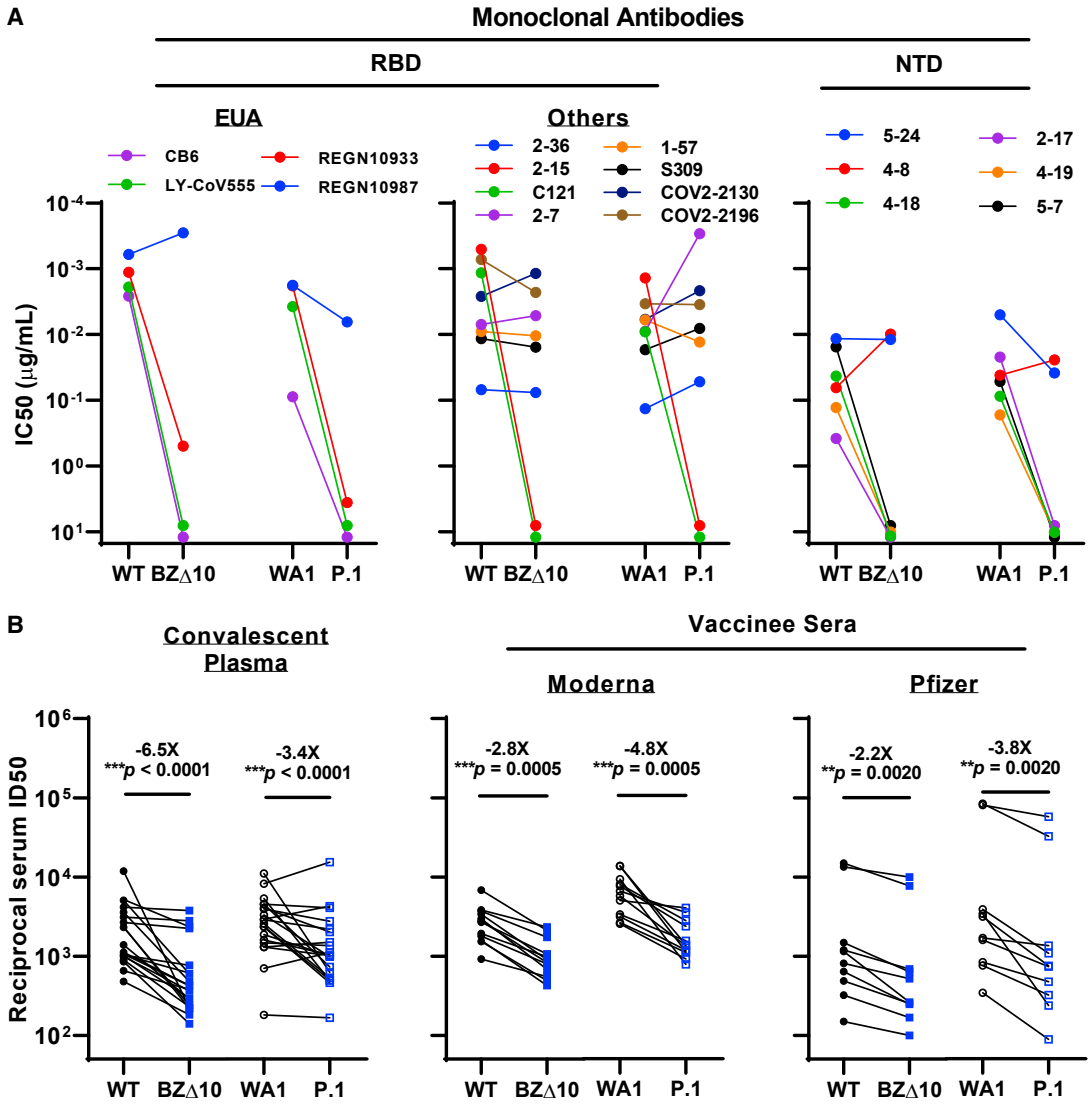

Figure 1. Neutralization of BZD10 and P.1 by mAbs, convalescent plasma, and vaccinee sera

(A) Changes in neutralization IC_{50} of select RBD and NTD mAbs.

(B) Changes in reciprocal plasma neutralization ID_{50} values of convalescent plasma and reciprocal serum ID_{50} values for persons who received Moderna or Pfizer vaccine. Mean fold change in ID_{50} relative to the WT is written above the p values. Statistical analysis was performed using a Wilcoxon matched-pairs signed rank test. Two-tailed p values are reported.

See also Figures S1.

B.1.351 (Wang et al., 2021), which should not be surprising since the triple RBD mutations in P.1 and B.1.351 are largely the same.

We also assessed the neutralizing activity of six NTD mAbs (Liu et al., 2020) against the P.1 pseudovirus and authentic virus (Figure 1A, right panel; Figure S1B). P.1 was profoundly resistant to neutralization by four NTD antibodies: 2-17, 4-18, 4-19, and 5-7. Interestingly, 5-24 and 4-8, two mAbs targeting the antigenic supersite in NTD (Cerutti et al., 2021) that have completely lost neutralizing activity against B.1.351 (Wang et al., 2021), remained active against P.1. To understand the specific mutations responsible for the observed pattern of neutralization, we then tested these NTD mAbs against a panel of pseudoviruses, each containing only a single NTD mutation found in P.1 (Figure S1B). As expected, 5-24 ad 4-8 retained activity against all single-mutation pseudoviruses. P26S only partially accounted for the loss of activity of 4-18; L18F, T20N, and D138Y contributed to the loss of activity of 2-17 and 4-19; and L18F, T20N, D138Y, and R190S together resulted in the loss of activity of 5-7.

We also examined a panel of convalescent plasma obtained from 20 SARS-CoV-2 patients infected in the spring of 2020, as previously reported (Wang et al., 2021). Each plasma sample was assayed for neutralization against the P.1 pseudovirus and authentic virus in parallel with their WT counterparts. As shown in Figure S1C, many samples lost >2-fold neutralizing activity against BZΔ10 and P.1. The magnitude of the drop in plasma

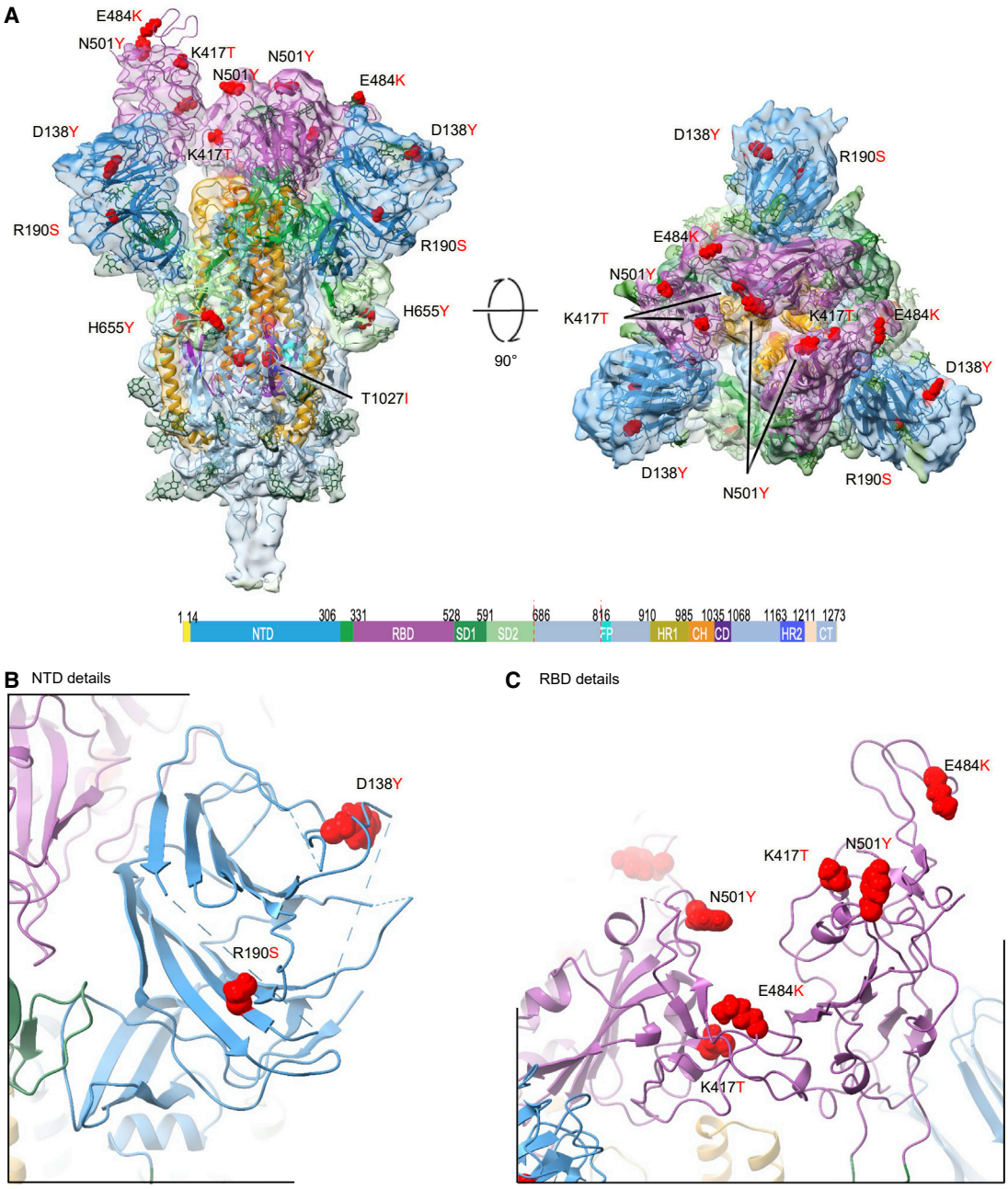

Figure 2. Cryo-EM structure of the P.1 spike

(A) Overall cryo-EM structure of the P.1 spike trimer with domains colored as shown in key, glycans shown in green, and mutations highlighted in red. Density is shown for the 3.8 Å reconstruction with the molecular model shown in ribbon representation. The left image shows a side view, with viral membrane located below, and the right image shows the view looking down on the spike apex.

(B) NTD close up view.

(C) RBD close up view.

See also Figure S2 and Table S1.

neutralization infectious dose $(ID)_{50}$ titers is summarized in Figure 1B (left panel), showing a 6.5-fold loss of activity against the variant pseudovirus and a 3.4-fold loss of activity against the authentic virus.

Twenty-two vaccinee sera were obtained, as previously reported (Wang et al., 2021), from 12 individuals who received Moderna SARS-Co-2 mRNA-1273 vaccine (Anderson et al., 2020) and 10 individuals who received the Pfizer BNT162b2 COVID-19 vaccine (Polack et al., 2020). Each serum sample was assayed for neutralization against BZΔ10 and P.1 together with WT viruses. The extent of the decline in neutralization activity is summarized in Figure 1B (middle and right panels), and

each neutralization profile is shown in Figure S1D. A loss of activity against BZΔ10 and P.1 was noted for every sample, but the magnitude of the loss was modest (2.2–2.8 fold for the pseudovirus; 3.8–4.8 fold for the authentic virus) and not as striking as was observed against B.1.351 (6.5–8.6 fold for pseudovirus; 10.3–12.4 fold for authentic virus) (Wang et al., 2021).

To provide insight into the mechanisms of antibody resistance, we determined the structure of the 2-proline-stabilized P.1 spike protein at 3.8 Å resolution by single-particle cryoelectron microscopy (cryo-EM) (Figures 2; Figure S2; Table S1). Overall, the structure of the P.1 spike was highly similar to the D614G variant (Korber et al., 2020; Yurkovetskiy et al., 2020), with 3D classes observed only for the single-RBD-up conformation. This was expected, as the D614G mutation, contained in P1, appears to favor the one-up orientation of RBD, which is required for ACE2 binding and recognition by some RBD-directed antibodies. Structural mobility was observed with the raised RBD (protomer B), but not with protomers A and C, which were in the down orientation (Video S1). Map density was well satisfied by the previously reported single-up structure (PDB: 6XM0) for the majority of the trimer, except in three regions. Residues 310–322 in protomer A traced a different path, residues 623–632 were disordered in protomers A and B and partially ordered in protomer C, and residues 828–853 were disordered in protomers A and C and partially ordered in protomer B. Notably, two of these regions around residues 320 and 840 were previously observed to "refold" between the single-up and the low-pH all-RBD-down conformation (Zhou et al., 2020), suggesting these regions are generally more mobile—and in this case, sensitive to mutation-induced conformational changes.

Because of the high overall conformational similarity to the D614G structure, we infer the functional impact of the P.1 mutation to arise primarily from local changes in structure. Other than H655Y and T1027I, all of the mutations occur within the NTD or RBD, which are the targets of neutralizing antibodies. For the NTD, the N terminus was disordered until residue 27, so we were unable to visualize mutations at residue 18, 20, and 26. Mutation D138Y is located in the center of the NTD supersite (Cerutti et al., 2021), explaining its impact on NTD antibodies 2-17 and 4-19 (Figure S1B), whereas R190S is mostly occluded from the NTD surface (Figure 2B). For RBD, the three mutations at K417T, E484K, and N501Y are all located in the ACE2-binding region and overlap epitopes for multiple neutralizing antibodies. Their relatively equal spatial separation (Figure 2C) allow them to impact a substantial portion of the ACE2-binding surface.

Overall, the SARS-CoV-2 P.1 variant is of concern because of its rapid rise to dominance as well as its extensive spike mutations, which could lead to antigenic changes detrimental to mAb therapies and vaccine protection. Here we report that P.1 is indeed resistant to neutralization by several RBD-directed mAbs, including three with EUA. The major culprit is the E484K mutation, which has emerged independently in over 50 lineages, including in B.1.526 that we (Annavajhala et al., 2021) and others (West et al., 2021) have identified in New York recently. As for the NTD-directed mAbs, the resistance profiles are markedly different between P.1 and B.1.351, reflecting their distinct sets of mutations in NTD. Both convalescent plasma and vaccinee sera show a significant loss of neutralizing activity against P.1, but the diminution is not as great as that reported against B.1.351 (Garcia-Beltran et al., 2021; Wang et al., 2021). Therefore, the threat of increased reinfection or decreased vaccine protection posed by P.1 may not be as severe as B.1.351. Finally, given that the RBD mutations are largely the same for these two variants, the discrepancy in their neutralization susceptibility to polyclonal plasma or sera suggests that NTD mutations can have a significant effect on the susceptibility of SARS-CoV-2 to antibody neutralization.

STAR★METHODS

Detailed methods are provided in the online version of this paper and include the following:

- KEY RESOURCES TABLE
- RESOURCE AVAILABILITY
  - Lead contact
  - Materials availability
  - Data and code availability
- EXPERIMENTAL MODEL AND SUBJECT DETAILS
  - Patients and vaccinees
  - Cell lines
- METHOD DETAILS
  - Monoclonal antibodies
  - Pseudovirus neutralization assays
  - Authentic SARS-CoV-2 microplate neutralization
  - Cryo-EM data collection and processing
  - Cryo-EM model building
- QUANTIFICATION AND STATISTICAL ANALYSIS

SUPPLEMENTAL INFORMATION

Supplemental information can be found online at https://doi.org/10.1016/j.chom.2021.04.007.

ACKNOWLEDGMENTS

The following reagent was obtained through BEI Resources, NIAID, NIH: SARS-Related Coronavirus 2, Isolate hCoV-19/Japan/TY7-503/2021 (Brazil P.1), NR-54982, contributed by National Institute of Infectious Diseases. We thank Bob Grassucci and Chi Wang for help with cryo-EM data collection at the Columbia University cryo-EM Center at the Zuckerman Institute. This study was supported by funding from Andrew and Peggy Cherng, Samuel Yin, Barbara Picower, and the JPB Foundation, Brii Biosciences, Roger and David Wu, and the Bill and Melinda Gates Foundation. Support was also provided by the Intramural Program of the Vaccine Research Center, National Institute of Allergy and Infectious Diseases, National Institutes of Health.

AUTHOR CONTRIBUTIONS

The study was conceptualized by D.D.H. The virology experiments were carried out by P.W., M.S.N., M.W., J.Y., L.L., and Y.H. The structural experiment were carried out by R.G.C., G.C., P.D.K., and L.S. The manuscript was written by P.W., R.G.C., P.D.K., L.S., and D.D.H. and reviewed, commented, and approved by all the authors.

DECLARATION OF INTERESTS

P.W., J.Y., M.N., Y.H., L.L., and D.D.H. are inventors on a provisional patent application on mAbs to SARS-CoV-2.

Received: March 8, 2021
Revised: March 31, 2021
Accepted: April 14, 2021
Published: April 18, 2021

REFERENCES

Adams, P.D., Gopal, K., Grosse-Kunstleve, R.W., Hung, L.W., Ioerger, T.R., McCoy, A.J., Moriarty, N.W., Pai, R.K., Read, R.J., Romo, T.D., et al. (2004). Recent developments in the PHENIX software for automated crystallographic structure determination. J. Synchrotron Radiat. *11*, 53–55.

Anderson, E.J., Rouphael, N.G., Widge, A.T., Jackson, L.A., Roberts, P.C., Makhene, M., Chappell, J.D., Denison, M.R., Stevens, L.J., Pruijssers, A.J., et al.; mRNA-1273 Study Group (2020). Safety and Immunogenicity of SARS-CoV-2 mRNA-1273 Vaccine in Older Adults. N. Engl. J. Med. *383*, 2427–2438.

Annavajhala, M.K., Mohri, H., Zucker, J.E., Sheng, Z., Wang, P., Gomez-Simmonds, A., Ho, D.D., and Uhlemann, A.-C. (2021). A Novel SARS-CoV-2 Variant of Concern, B.1.526, Identified in New York. medRxiv. https://doi.org/10.1101/2021.02.23.21252259.

Cerutti, G., Guo, Y., Zhou, T., Gorman, J., Lee, M., Rapp, M., Reddem, E.R., Yu, J., Bahna, F., Bimela, J., et al. (2021). Potent SARS-CoV-2 neutralizing antibodies directed against spike N-terminal domain target a single supersite. Cell Host Microbe j.chom.2021.03.005.

Chen, P., Nirula, A., Heller, B., Gottlieb, R.L., Boscia, J., Morris, J., Huhn, G., Cardona, J., Mocherla, B., Stosor, V., et al.; BLAZE-1 Investigators (2021). SARS-CoV-2 Neutralizing Antibody LY-CoV555 in Outpatients with Covid-19. N. Engl. J. Med. *384*, 229–237.

Croll, T.I. (2018). ISOLDE: a physically realistic environment for model building into low-resolution electron-density maps. Acta Crystallogr. D Struct. Biol. *74*, 519–530.

Davis, I.W., Murray, L.W., Richardson, J.S., and Richardson, D.C. (2004). MOLPROBITY: structure validation and all-atom contact analysis for nucleic acids and their complexes. Nucleic Acids Res. *32*, W615-9.

Emsley, P., and Cowtan, K. (2004). Coot: model-building tools for molecular graphics. Acta Crystallogr. D Biol. Crystallogr. *60*, 2126–2132.

Faria, N.R. (2021). Genomic characterisation of an emergent SARS-CoV-2 lineage in Manaus: preliminary findings. Published January 12, 2021 https://virological.org/t/genomic-characterisation-of-an-emergent-sars-cov-2-lineage-in-manaus-preliminary-findings/586.

Garcia-Beltran, W.F., Lam, E.C., Denis, K.S., Nitido, A.D., Garcia, Z.H., Hauser, B.M., Feldman, J., Pavlovic, M.N., Gregory, D.J., Poznansky, M.C., et al. (2021). Circulating SARS-CoV-2 variants escape neutralization by vaccine-induced humoral immunity. medRxiv. https://doi.org/10.1101/2021.02.14.21251704.

Goddard, T.D., Huang, C.C., Meng, E.C., Pettersen, E.F., Couch, G.S., Morris, J.H., and Ferrin, T.E. (2018). UCSF ChimeraX: Meeting modern challenges in visualization and analysis. Protein Sci. *27*, 14–25.

Gottlieb, R.L., Nirula, A., Chen, P., Boscia, J., Heller, B., Morris, J., Huhn, G., Cardona, J., Mocherla, B., Stosor, V., et al. (2021). Effect of Bamlanivimab as Monotherapy or in Combination With Etesevimab on Viral Load in Patients With Mild to Moderate COVID-19: A Randomized Clinical Trial. JAMA *325*, 632–644.

Hansen, J., Baum, A., Pascal, K.E., Russo, V., Giordano, S., Wloga, E., Fulton, B.O., Yan, Y., Koon, K., Patel, K., et al. (2020). Studies in humanized mice and convalescent humans yield a SARS-CoV-2 antibody cocktail. Science *369*, 1010–1014.

Korber, B., Fischer, W.M., Gnanakaran, S., Yoon, H., Theiler, J., Abfalterer, W., Hengartner, N., Giorgi, E.E., Bhattacharya, T., Foley, B., et al. (2020). Tracking Changes in SARS-CoV-2 Spike: Evidence that D614G Increases Infectivity of the COVID-19 Virus. Cell *182*, 812–827.e19.

Liu, L., Wang, P., Nair, M.S., Yu, J., Rapp, M., Wang, Q., Luo, Y., Chan, J.F., Sahi, V., Figueroa, A., et al. (2020). Potent neutralizing antibodies against multiple epitopes on SARS-CoV-2 spike. Nature *584*, 450–456.

Liu, Y., Liu, J., Xia, H., Zhang, X., Fontes-Garfias, C.R., Swanson, K.A., Cai, H., Sarkar, R., Chen, W., Cutler, M., et al. (2021). Neutralizing Activity of BNT162b2-Elicited Serum - Preliminary Report. N. Engl. J. Med. *384*, 1466–1468.

Mastronarde, D.N. (2005). Automated electron microscope tomography using robust prediction of specimen movements. J. Struct. Biol. *152*, 36–51.

Naveca, F. (2021). Phylogenetic relationship of SARS-CoV-2 sequences from Amazonas with emerging Brazilian variants harboring mutations E484K and N501Y in the Spike protein. Published on January 12, 2021 https://virological.org/t/phylogenetic-relationship-of-sars-cov-2-sequences-from-amazonas-with-emerging-brazilian-variants-harboring-mutations-e484k-and-n501y-in-the-spike-protein/585.

Pettersen, E.F., Goddard, T.D., Huang, C.C., Couch, G.S., Greenblatt, D.M., Meng, E.C., and Ferrin, T.E. (2004). UCSF Chimera–a visualization system for exploratory research and analysis. J. Comput. Chem. *25*, 1605–1612.

Pinto, D., Park, Y.-J., Beltramello, M., Walls, A.C., Tortorici, M.A., Bianchi, S., Jaconi, S., Culap, K., Zatta, F., De Marco, A., et al. (2020). Cross-neutralization of SARS-CoV-2 by a human monoclonal SARS-CoV antibody. Nature *583*, 290–295.

Polack, F.P., Thomas, S.J., Kitchin, N., Absalon, J., Gurtman, A., Lockhart, S., Perez, J.L., Pérez Marc, G., Moreira, E.D., Zerbini, C., et al.; C4591001 Clinical Trial Group (2020). Safety and Efficacy of the BNT162b2 mRNA Covid-19 Vaccine. N. Engl. J. Med. *383*, 2603–2615.

Punjani, A., Rubinstein, J.L., Fleet, D.J., and Brubaker, M.A. (2017). cryoSPARC: algorithms for rapid unsupervised cryo-EM structure determination. Nat. Methods *14*, 290–296.

Robbiani, D.F., Gaebler, C., Muecksch, F., Lorenzi, J.C.C., Wang, Z., Cho, A., Agudelo, M., Barnes, C.O., Gazumyan, A., Finkin, S., et al. (2020). Convergent antibody responses to SARS-CoV-2 in convalescent individuals. Nature *584*, 437–442.

Shi, R., Shan, C., Duan, X., Chen, Z., Liu, P., Song, J., Song, T., Bi, X., Han, C., Wu, L., et al. (2020). A human neutralizing antibody targets the receptor-binding site of SARS-CoV-2. Nature *584*, 120–124.

Tegally, H., Wilkinson, E., Giovanetti, M., Iranzadeh, A., Fonseca, V., Giandhari, J., Doolabh, D., Pillay, S., San, E.J., Msomi, N., et al. (2021). Detection of a SARS-CoV-2 variant of concern in South Africa. Nature *592*, 438–443.

Wang, P., Liu, L., Nair, M.S., Yin, M.T., Luo, Y., Wang, Q., Yuan, T., Mori, K., Solis, A.G., Yamashita, M., et al. (2020). SARS-CoV-2 neutralizing antibody responses are more robust in patients with severe disease. Emerg. Microbes Infect. *9*, 2091–2093.

Wang, P., Nair, M.S., Liu, L., Iketani, S., Luo, Y., Guo, Y., Wang, M., Yu, J., Zhang, B., Kwong, P.D., et al. (2021). Antibody resistance of SARS-CoV-2 variants B.1.351 and B.1.1.7. Nature. https://doi.org/10.1038/s41586-021-03398-2.

West, A.P., Jr., Barnes, C.O., Yang, Z., and Bjorkman, P.J. (2021). SARS-CoV-2 lineage B.1.526 emerging in the New York region detected by software utility created to query the spike mutational landscape. bioRxiv. https://doi.org/10.1101/2021.02.14.431043.

Wu, K., Werner, A.P., Koch, M., Choi, A., Narayanan, E., Stewart-Jones, G.B.E., Colpitts, T., Bennett, H., Boyoglu-Barnum, S., Shi, W., et al. (2021). Serum Neutralizing Activity Elicited by mRNA-1273 Vaccine - Preliminary Report. N. Engl. J. Med. *384*, 1468–1470.

Yurkovetskiy, L., Wang, X., Pascal, K.E., Tomkins-Tinch, C., Nyalile, T.P., Wang, Y., Baum, A., Diehl, W.E., Dauphin, A., Carbone, C., et al. (2020). Structural and Functional Analysis of the D614G SARS-CoV-2 Spike Protein Variant. Cell *183*, 739–751.e8.

Zhou, T., Tsybovsky, Y., Gorman, J., Rapp, M., Cerutti, G., Chuang, G.-Y., Katsamba, P.S., Sampson, J.M., Schön, A., Bimela, J., et al. (2020). Cryo-EM Structures of SARS-CoV-2 Spike without and with ACE2 Reveal a pH-Dependent Switch to Mediate Endosomal Positioning of Receptor-Binding Domains. Cell Host Microbe *28*, 867–879.e5.

Zost, S.J., Gilchuk, P., Case, J.B., Binshtein, E., Chen, R.E., Nkolola, J.P., Schäfer, A., Reidy, J.X., Trivette, A., Nargi, R.S., et al. (2020). Potently neutralizing and protective human antibodies against SARS-CoV-2. Nature *584*, 443–449.

STAR★METHODS

KEY RESOURCES TABLE

REAGENT or RESOURCE	SOURCE	IDENTIFIER
Antibodies		
2-36	Liu et al., 2020	N/A
2-15	Liu et al., 2020	N/A
2-7	Liu et al., 2020	N/A
1-57	Liu et al., 2020	N/A
4-8	Liu et al., 2020	N/A
4-18	Liu et al., 2020	N/A
5-24	Liu et al., 2020	N/A
2-17	Liu et al., 2020	N/A
4-19	Liu et al., 2020	N/A
5-7	Liu et al., 2020	N/A
REGN10987	Hansen et al., 2020	N/A
REGN10933	Hansen et al., 2020	N/A
LY-CoV555	Chen et al., 2021	N/A
CB6	Shi et al., 2020	N/A
C121	Robbiani et al., 2020	N/A
S309	Pinto et al., 2020	N/A
COV2-2130	Zost et al., 2020	N/A
COV2-2196	Zost et al., 2020	N/A
Bacterial and virus strains		
VSV-G pseudo-typed DG-luciferase	Kerafast	Cat# EH1020-PM
WA1 (SARS-Related Coronavirus 2, Isolate USA-WA1/2020)	BEI Resources	Cat# NR-52281
P.1 (SARS-Related Coronavirus 2, Isolate hCoV-19/Japan/TY7-503/2021)	BEI Resources	Cat# NR-54982
Biological samples		
Convalescent human plasma samples	Columbia University Irving Medical Center	N/A
Serum samples from Pfizer BNT162b2 Covid-19 Vaccine trial	Columbia University Irving Medical Center	N/A
Serum samples from Moderna SARS-CoV-2 mRNA-1273 Vaccine Phase 1 clinical trial	NIH	N/A
Chemicals, peptides, and recombinant proteins		
n-Dodecyl-b-D-Maltopyranoside	Anatrace	Cat# D310
HEPES	Sigma	Cat# H3375
NaCl	Sigma	Cat# S9888
Critical commercial assays		
FuGENE 6	Promega	Cat# E2691
Quikchange II XL site-directed mutagenesis kit	Agilent	Cat# 200522
Luciferase Assay System	Promega	Cat# E1501
Experimental models: cell lines		
Vero E6	ATCC	Cat# CRL-1586
HEK293T/17	ATCC	Cat# CRL-11268
I1 mouse hybridoma	ATCC	Cat# CRL-2700

(*Continued on next page*)

Continued

REAGENT or RESOURCE	SOURCE	IDENTIFIER
Recombinant DNA		
pCMV3-SARS-CoV-2-spike D614G	Wang et al., 2021	N/A
pCMV3-SARS-CoV-2-spike L18F	Wang et al., 2021	N/A
pCMV3-SARS-CoV-2-spike T20N	This study	N/A
pCMV3-SARS-CoV-2-spike P26S	This study	N/A
pCMV3-SARS-CoV-2-spike D138Y	This study	N/A
pCMV3-SARS-CoV-2-spike R190S	This study	N/A
pCMV3-SARS-CoV-2-spike BZD10	This study	N/A
Deposited data		
Cryo-EM structure of SARS-CoV-2 variant P.1 spike glycoprotein	This study	PDB: 7M8K EMDB: EMD-23718
Sequence of hCoV-19/Japan/TY7-503/2021 (P.1)	GISAID	EPI_ISL_877769
Additional Supplemental Items are available from Mendeley Data at https://doi.org/10.17632/r5v4jj5hyz.1	This study	N/A
Software and algorithms		
GraphPad Prism Software	GraphPad Prism Software, Inc.	N/A
SerialEM	Mastronarde, 2005	https://bio3d.colorado.edu/SerialEM/
cryoSPARC	Punjani et al., 2017	https://cryosparc.com
UCSF Chimera	Pettersen et al., 2004	https://www.cgl.ucsf.edu/chimera/
UCSF Chimera X	Goddard et al., 2018	https://www.cgl.ucsf.edu/chimerax/
ISOLDE	Croll, 2018	https://isolde.cimr.cam.ac.uk/
Phenix	Adams et al., 2004	https://www.phenix-online.org
Coot	Emsley and Cowtan, 2004	https://www2.mrc-lmb.cam.ac.uk/personal/pemsley/coot
Molprobity	Davis et al., 2004	http://molprobity.biochem.duke.edu

RESOURCE AVAILABILITY

Lead contact

Further information and requests for resources and reagents should be directed to and will be fulfilled by the Lead Contact Author David D. Ho (dh2994@cumc.columbia.edu).

Materials availability

All unique/stable reagents generated in this study are available from the Lead Contact with a completed Materials Transfer Agreement.

Data and code availability

Cryo-EM structure of SARS-CoV-2 variant P.1 spike glycoprotein have been deposited in the PDB (7M8K) and EMDB (EMD-23718). The sequence of hCoV-19/Japan/TY7-503/2021 (P.1) virus is available in the GISAID database (EPI_ISL_877769).

EXPERIMENTAL MODEL AND SUBJECT DETAILS

Patients and vaccinees

Convalescent plasma and vaccinee sera were the same as previously reported (Wang et al., 2021). Plasma samples were obtained from patients (mean age: 53, range: 29-79; 65% male) convalescing from documented SARS-CoV-2 infection approximately one month after recovery or later. These cases were enrolled into an observational cohort study of convalescent patients followed at the Columbia University Irving Medical Center (CUIMC) starting in the Spring of 2020. The study protocol was approved by the CUIMC Institutional Review Board (IRB), and all participants provided written informed consent. Sera were obtained from 12 participants in a Phase 1 clinical trial of Moderna SARS-CoV-2 mRNA-1273 Vaccine conducted at the NIH, under a NIH IRB-approved protocol (Anderson et al., 2020), 4 subjects each from cohorts 2, 5 and 8 (100 μg across the age spectra, 18-55, 56-70, > 70 YOA). Sera

were also obtained from 10 individuals (mean age: 42, range: 29-64; 50% male) followed in a CUIMC IRB-approved protocol to assess immunological responses to SARS-CoV-2 who received the Pfizer BNT162b2 Covid-19 Vaccine as a part of the emergency use authorization.

Cell lines

HEK293T/17 (cat# CRL-11268) and Vero E6 cells (cat# CRL-1586) were from ATCC and cultured in 10% Fetal Bovine Serum (FBS, GIBCO cat# 16140071) supplemented Dulbecco's Modified Eagle Medium (DMEM, ATCC cat# 30-2002) at 37°C, 5% CO_2. I1 mouse hybridoma cells (ATCC, cat# CRL-2700) were cultured in Eagle's Minimum Essential Medium (EMEM, ATCC cat# 30-2003)) with 20% FBS.

METHOD DETAILS

Monoclonal antibodies

Monoclonal antibodies tested in this study were constructed and produced at Columbia University as previously described (Liu et al., 2020; Wang et al., 2021), except REGN10933, REGN10987, COV2-2196, and COV2-2130 were provided by Regeneron Pharmaceuticals, Inc., and CB6 was provided by P.D.K.

Pseudovirus neutralization assays

Plasmids encoding the single-mutation variants found in P.1 and 10-mutation variant (BZD10) were generated by Quikchange II XL site-directed mutagenesis kit (Agilent). Recombinant Indiana VSV (rVSV) expressing different SARS-CoV-2 spike variants were generated as previously described (Liu et al., 2020; Wang et al., 2020; Wang et al., 2021). Briefly, HEK293T cells were grown to 80% confluency before transfection with the spike gene using Lipofectamine 3000 (Invitrogen). Cells were cultured overnight at 37°C with 5% CO_2, and VSV-G pseudo-typed DG-luciferase (G*DG-luciferase, Kerafast) was used to infect the cells in DMEM at an MOI of 3 for 2 h before washing the cells with 1X DPBS three times. The next day, the transfection supernatant was harvested and clarified by centrifugation at 300 g for 10 min. Each viral stock was then incubated with 20% I1 hybridoma (anti-VSV-G, ATCC: CRL-2700) supernatant for 1 h at 37°C to neutralize contaminating VSV-G pseudo-typed DG-luciferase virus before measuring titers and making aliquots to be stored at −80°C.

Neutralization assays were performed by incubating pseudoviruses with serial dilutions of mAbs or heat-inactivated plasma or sera, and scored by the reduction in luciferase gene expression as previously described (Liu et al., 2020; Wang et al., 2020; Wang et al., 2021). Briefly, Vero E6 cells (ATCC) were seeded in 96-well plates (2×10^4 cells per well). Pseudoviruses were incubated with serial dilutions of the test samples in triplicate for 30 min at 37 °C. The mixture was added to cultured cells and incubated for an additional 16 h. Luminescence was measured using Luciferase Assay System (Promega), and IC_{50} was defined as the dilution at which the relative light units were reduced by 50% compared with the virus control wells (virus + cells) after subtraction of the background in the control groups with cells only. The IC_{50} values were calculated using a five-parameter dose-response curve in GraphPad Prism.

Authentic SARS-CoV-2 microplate neutralization

The SARS-CoV-2 viruses USA-WA1/2020 (WA1), and hCoV-19/Japan/TY7-503/2021 (P.1) were obtained from BEI Resources (NIAID, NIH). The deposited virus (Passage 2 in Vero E6/TMPRSS2 cells) was reported to have an additional mutation as compared to the clinical isolate: NSP6 (Non-structural protein 6) F184V (GISAID: EPI_ISL_877769). The viruses were propagated for one passage using Vero E6 cells. Virus infectious titer was determined by an end-point dilution and cytopathic effect (CPE) assay on Vero E6 cells as described previously (Liu et al., 2020; Wang et al., 2020; Wang et al., 2021).

An end-point-dilution microplate neutralization assay was performed to measure the neutralization activity of convalescent plasma samples, vaccinee sera, and purified mAbs. Triplicates of each dilution were incubated with SARS-CoV-2 at an MOI of 0.1 in EMEM with 7.5% inactivated fetal calf serum (FCS) for 1 h at 37°C. Post incubation, the virus-antibody mixture was transferred onto a monolayer of Vero E6 cells grown overnight. The cells were incubated with the mixture for ~70 h. CPE was visually scored for each well in a blinded fashion by two independent observers. The results were then converted into percentage neutralization at a given sample dilution or mAb concentration, and the averages ± SEM were plotted using a five-parameter dose-response curve in GraphPad Prism.

Cryo-EM data collection and processing

2 μL P.1 spike protein at a concentration of 1 mg/mL buffered with 10 mM HEPES pH 7.4, 150 mM NaCl, and 0.005% n-dodecyl-b-D-maltoside (DDM) was incubated on C-flat 1.2/1.3 carbon grids for 30 s and vitrified using a Vitrobot Mark IV plunge freezer. Data was collected on a Titan Krios electron microscope operating at 300 kV, equipped with a Gatan K3 direct electron detector and energy filter, using the SerialEM software package (Mastronarde, 2005). A total electron fluence of 41.92 e-/Å2 was fractionated over 60 frames, with a total exposure time of 3.0 s. A magnification of 81,000x resulted in a pixel size of 1.07 Å, and a defocus range of −0.5 to −2.5 μm was used.

All processing was done using cryoSPARC v3.2.0 (Punjani et al., 2017). Raw movies were aligned and dose-weighted using patch motion correction, and the CTF was estimated using patch CTF estimation. Micrographs were picked using blob picker, and a particle set was selected using 2D and 3D classification. Selected particle picks were manually curated for a small randomized subset of

approximately 300 micrographs and used to train a Topaz neural network. This network was then used to pick particles from the remaining micrographs, which were extracted with a box size of 384 pixels. The resulting particle set was refined to high resolution using a combination of heterogenous and homogeneous refinement, followed by nonuniform refinement. The final map was submitted to the EMDB with ID: EMD-23718.

Cryo-EM model building

We used PDB 6XM0, one of the most complete coronavirus spike structures, as a starting model. The model was docked to the map using Chimera (Pettersen et al., 2004), and then fitted interactively using ISOLDE (Croll, 2018) and COOT (Emsley and Cowtan, 2004). Real space refinement was performed in Phenix 1.18 (Adams et al., 2004). Validation was performed using Molprobity (Davis et al., 2004). The model was submitted to the PDB with PDB ID: 7M8K. Figures were prepared using UCSF ChimeraX (Goddard et al., 2018).

QUANTIFICATION AND STATISTICAL ANALYSIS

The statistical analyses for the pseudovirus and authentic virus neutralization assessments were performed using GraphPad Prism for calculation of mean value and SEM for each data point (see Figure S1). Each specimen was tested in triplicate. Antibody neutralization IC_{50} values were calculated using a five-parameter dose-response curve in GraphPad Prism (see Figure 1). For comparing the plasma/serum neutralization titers, statistical analysis was performed using a Wilcoxon matched-pairs signed rank test. Two-tailed p values are reported. No statistical methods were used to determine whether the data met assumptions of the statistical approach. Cryo-EM data was processed and analyzed using cryoSPARC and Chimera (see Figures 2; Figure S2). Structural model statistics were analyzed using ISOLDE, Phenix, Coot, and Molprobity (see Table S1). Statistical details of experiments are described in Method Details or Figure Legends.